



**HAL**  
open science

# Design Considerations of a CMOS Envelope Detector for Low Power Wireless Receiver Applications

Jack Ou, Pietro Maris Ferreira

► **To cite this version:**

Jack Ou, Pietro Maris Ferreira. Design Considerations of a CMOS Envelope Detector for Low Power Wireless Receiver Applications. New Circuits and Systems Conference (NEWCAS), 2017 15th IEEE International, Jun 2017, Strasbourg, France. 10.1109/newcas.2017.8010148 . hal-01657109

**HAL Id: hal-01657109**

**<https://hal.science/hal-01657109v1>**

Submitted on 13 Oct 2022

**HAL** is a multi-disciplinary open access archive for the deposit and dissemination of scientific research documents, whether they are published or not. The documents may come from teaching and research institutions in France or abroad, or from public or private research centers.

L'archive ouverte pluridisciplinaire **HAL**, est destinée au dépôt et à la diffusion de documents scientifiques de niveau recherche, publiés ou non, émanant des établissements d'enseignement et de recherche français ou étrangers, des laboratoires publics ou privés.

# Design Considerations of a CMOS Envelope Detector for Low Power Wireless Receiver Applications

Jack Ou  
 Department of Electrical and Computer Engineering  
 California State University Northridge  
 Northridge, California 91330-8346  
 Email: jack.ou@csun.edu

Pietro M. Ferreira  
 GeePs (UMR CNRS 8507)  
 CentraleSuplec, Université Paris-Saclay  
 Gif-sur-Yvette, France  
 Email: maris@ieee.org

**Abstract**—Previous studies have shown that a transistor’s transconductance-to-drain-current ratio is useful for optimizing analog circuits. In this paper, we derive an expression that captures the second order distortion generated at the output of an envelope detector. We use the derived expression, along with the nonlinear Taylor series coefficients to design a 3  $\mu\text{A}$  envelope detector in 0.13  $\mu\text{m}$  CMOS process.

## I. INTRODUCTION

Nanoscale Metal Oxide Field Effect Transistor (MOSFET) circuit design is driven by power consumption constraints. In 1996, Silveira *et al.* proposed a powerful transconductance-to-drain current ( $g_m/I_D$ ) method to help designers size up transistors quickly [1]. The so called “ $g_m/I_D$  design approach” was originally developed to calculate parameters such as small signal gain and bandwidth [1] and later extended to distortion analysis [2].

A procedure to model a transistor’s nonlinearity using  $g_m/I_D$  dependent Taylor series coefficients was described in [2]. Analytical expressions that link a transistor’s distortion to its own  $g_m/I_D$  were discussed in [3] and further explored in [4].

In this paper, instead of seeking to minimize distortion, we use distortion to optimize the gain of an envelope detector. Section II reviews the fundamentals of  $g_m/I_D$  dependent Taylor series coefficients. Section III derives an expression that captures the second order distortion current generated at the output of an envelope detector. Section IV explores the design space of an envelope detector and discusses the design trade-offs of a 3  $\mu\text{A}$  envelope detector. Section V summarizes the results and explores the limitations of the described technique.

## II. THEORY

### A. $g_m/I_D$ Dependent Taylor Series Coefficients

There are two types of nonlinear behaviors in circuits: hard nonlinearity and soft nonlinearity [5]. Hard nonlinearity is present when the input voltage becomes too large and clipping occurs at the output. The distortion caused by hard nonlinearity is very large. Few applications can tolerate hard nonlinearity. This paper focuses instead on circuits that exhibit primarily characteristics of soft nonlinearity.

Devices that exhibit soft (weakly) nonlinear behavior can be described by means of a power series. For a weakly nonlinear MOS transistor, the drain-to-source current ( $i_{ds}$ ) is a function of the gate-to-source voltage ( $v_{gs}$ ) and the drain-to-source voltage ( $v_{ds}$ ) and can be written as a two-dimensional Taylor series approximation [6]:

$$i_{ds}(v_{gs}, v_{ds}) = g_{m1}v_{gs} + g_{ds1}v_{ds} + g_{m2}v_{gs}^2 + g_{ds2}v_{ds}^2 + x_{11}v_{gs}v_{ds} + g_{m3}v_{gs}^3 + g_{ds3}v_{ds}^3 + x_{12}v_{gs}v_{ds}^2 + x_{21}v_{gs}^2v_{ds} \quad (1)$$

where the Taylor coefficients ( $g_{mk}$ ,  $g_{dsk}$ , and  $x_{pq}$ ) are derived from the derivatives of  $I_{DS}$ .

$g_{mk}$  is proportional to the derivatives of  $I_{DS}$  with respect to  $V_{GS}$  and is defined as,

$$g_{mk} = \frac{1}{k!} \frac{\partial^k I_{DS}}{\partial V_{GS}^k}. \quad (2)$$

For instance,  $g_{m1}$  (i.e. the transconductance) is the first derivative of  $I_{DS}$  with respect to  $V_{GS}$  ( $g_{m1}$ ) and  $g_{m2}$  is twice the derivative of  $g_{m1}$  with respect to  $V_{GS}$ .

$g_{dsk}$  represents the derivatives of  $I_{DS}$  with respect to  $V_{DS}$  and is defined as,

$$g_{dsk} = \frac{1}{k!} \frac{\partial^k I_{DS}}{\partial V_{DS}^k}. \quad (3)$$

$g_{ds1}$ , for example, is the drain-to-source transconductance.

It is interesting to note that  $i_{ds}$  depends not only on the powers of  $v_{gs}$  and  $v_{ds}$ , but also on cross-terms such as  $x_{pq}$  which are defined as follows:

$$x_{pq} = \frac{1}{p!q!} \frac{\partial^{p+q} I_{DS}}{\partial V_{GS}^p \partial V_{DS}^q} \quad (4)$$

The cross-term  $x_{11}$ , for example, represents the dependence of the transconductance on the drain-source bias voltage and can become significant at high  $g_m/I_D$ .  $x_{12}$  and  $x_{21}$  are higher order derivatives of  $x_{11}$ .

It was shown in [2] that  $g_{mk}$ ,  $g_{dsk}$ , and  $x_{pq}$  are proportional to transistor width ( $W$ ). Consequently, a ratio formed by any

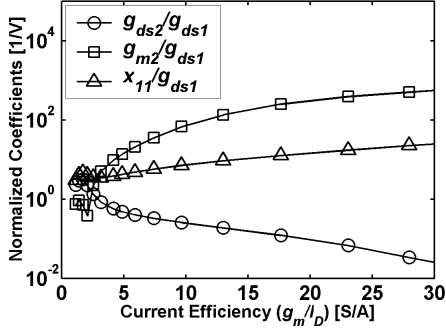


Fig. 1.  $g_m/I_D$  dependent ratios formed by two Taylor series coefficients.  $I_D = 0.5\mu\text{A}$ .  $L = 600\text{ nm}$ .  $V_{DS} = 0.6\text{ V}$ .  $V_{SB} = 0\text{ V}$ .

two Taylor series coefficients (e.g.  $g_{m2}/g_{ds1}$ ) is  $W$  independent and depends only on the  $g_m/I_D$  of a transistor. Figure 1 shows a collection of  $g_m/I_D$  dependent ratios of Taylor series coefficients from a  $0.13\ \mu\text{m}$  CMOS process.  $g_{m2}$ ,  $g_{ds2}$  and  $x_{11}$  are normalized to  $g_{ds1}$  in order to facilitate comparison of second order Taylor series coefficients. Figure 1 shows that for  $g_m/I_D > 10\text{ S/A}$ ,  $g_{m2}/g_{ds1} > x_{11}/g_{ds1} > g_{ds2}/g_{ds1}$ , i.e.  $g_{m2}$  is a significant contributor of second order nonlinearity.

### III. ANALYSIS

#### A. Qualitative Understanding of an Envelope Detector

Envelope detectors are frequently used in wireless receivers. Similar to elementary amplifiers, envelope detectors can be categorized as common-drain [8], common-gate [9], and common-source [7] envelope detectors. With the exception of the common-source envelope detector, the source terminal is used either as an input or as an output of the envelope detector. The source terminal carries a non-zero bias voltage. A three-dimensional Taylor series coefficient must be used [10] to capture a transistor's nonlinear dependence on source-to-body voltage ( $v_{sb}$ ). It can be challenging mathematically to analyze an envelope detector using a three-dimensional Taylor series.

In this paper, we focus instead on a common-source envelope detector with zero  $V_{SB}$  shown in Figure 2. We use  $g_m/I_D$  dependent two-dimensional Taylor series coefficient to model transistors' nonlinearity. The operation of the envelope detector can be understood as follows. A single tone at  $f_{in}$  is coupled to  $v_{in}$ . The second-order nonlinear parameters of  $M_1$  produces an *upconverted* tone at  $2f_{in}$  and a *downconverted* tone at DC at  $v_{op}$ . The DC current of  $M_3$  produces a DC voltage at  $v_{on}$ . The output is taken differentially in order to remove the DC component from  $v_{op}$ . The upconverted tone and the tone at  $f_{in}$  are removed from the desirable signal, i.e. the downconverted tone at DC, with the capacitor across the outputs.

#### B. Circuit Analysis

As will be shown in Sec. V-A,  $M_1$  is primarily responsible for the nonlinear operation of the envelope detector. Therefore, Fig. 3a can be used to approximate the behavior of the envelope detector. Fig. 3a can be further simplified to Fig.

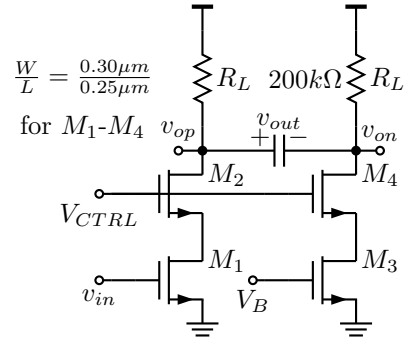


Fig. 2. Schematic of an envelope detector.

3b by recognizing that the resistance looking into the source  $M_2$  is  $R_X$ , where  $R_X$  is

$$R_X = \frac{r_{o,2} + R_L}{1 + (g_{m,2} + g_{mb,2})r_{o,2}}. \quad (5)$$

where  $g_{m,2}$ ,  $g_{mb,2}$ ,  $r_{o,2}$  are the transconductance, body transconductance and the output resistance of  $M_2$ .

Using (1) and expressing  $v_{ds}$  in a Taylor series approximation of  $v_{gs}$  [2],  $i_{ds,2nl}$ , the second order distortion of  $i_{ds}$  can be approximated as

$$i_{ds,2nl} = -(g_{m2,1} + g_{ds2,1}c_1^2 + x_{11,1}c_1)v_{in}^2, \quad (6)$$

where  $g_{m2,1}$ ,  $g_{ds2,1}$  and  $x_{11,1}$  are  $g_{m2}$ ,  $g_{ds2}$  and  $x_{11}$  of  $M_1$ .  $c_1$  is equal to  $-g_{m,1}(R_X || r_{o,1})$  and is the self-gain of  $M_1$ .

$i_{ds,2nl}$  is generated by  $M_1$  and is converted into a voltage at  $v_{op}$  by  $R_L$ . It can be shown that if  $v_{in} = v_m \cos(\omega_{in}t)$ , the second order tones generated at  $v_{op}$  are equal to

$$v_{op,2nl} = -R_L(i_{ds,2nl,g_{m2,1}} + i_{ds,2nl,g_{ds2,1}} + i_{ds,2nl,x_{11,1}}), \quad (7)$$

where

$$i_{ds,2nl,g_{m2,1}} = g_{m2,1} \frac{v_m^2}{2} \quad (8)$$

$$i_{ds,2nl,g_{ds2,1}} = g_{ds2,1} c_1^2 \frac{v_m^2}{2} \quad (9)$$

$$i_{ds,2nl,x_{11,1}} = x_{11,1} c_1 \frac{v_m^2}{2} \quad (10)$$

$i_{ds,2nl,g_{m2,1}}$ ,  $i_{ds,2nl,g_{ds2,1}}$ , and  $i_{ds,2nl,x_{11,1}}$  are second order distortion of  $i_{ds}$  due to  $g_{m2,1}$ ,  $g_{ds2,1}$  and  $x_{11,1}$ .

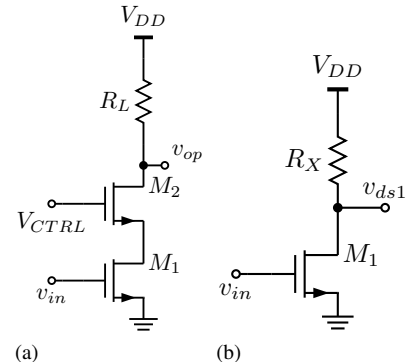


Fig. 3. (a) Equivalent circuit for the envelope detector in Fig. 2. (b) Equivalent circuit for analyzing distortion of  $M_1$ .

#### IV. DESIGN

The analysis in Sec.III shows that the envelope detector accomplishes spectrum translation through the second order nonlinearity of  $M_1$ , which is governed by the selection of  $L_1$ ,  $g_{m1,1}/I_{D,1}$  and  $I_{D,1}$ . In this section, we describe considerations that influence the selection of  $L_1$ ,  $g_{m1,1}/I_{D,1}$  and  $I_{D,1}$ .

##### A. Choice of $L_1$ and $I_{D,1}$

We start exploring the design space of  $L_1$  by assuming that  $I_{D,1}$  is  $5 \mu\text{A}$ . Figure 4a-4b suggest that both speed ( $f_T$ ) and current density are increased as  $L_1$  is reduced. Thus, assuming that  $I_{D,1}$  is constant,  $W_1$  is reduced as  $L_1$  is reduced (Fig. 4c).

For  $0.13 \mu\text{m}$  CMOS, the minimum width allowed by the design kit is  $280 \text{ nm}$ . Figure 4b shows that the current density at  $L = 250 \text{ nm}$  is  $5 \mu\text{A}/\mu\text{m}$ . Using a current density of  $5 \mu\text{A}/\mu\text{m}$ ,  $W_1$  (the width of  $M_1$ ) as a function of  $I_{D,1}$  is plotted in Fig. 4d. Figure 4d suggests that  $I_{D,1}$  should exceed or equal to  $1.5 \mu\text{A}$  if  $W_1$  were to exceed the minimum width permitted by the  $0.13 \mu\text{m}$  design kit.

##### B. Choice of $g_m/I_D$

Section III shows that  $i_{ds,2nl}$  is determined by  $g_{m2,1}$ ,  $g_{ds2,1}$ , and  $x_{11,1}$ . Therefore, the design space for  $g_m/I_D$  of  $M_1$  (i.e.  $g_{m1,1}/I_{D,1}$ ) should be explored. Figure 5 shows the dependence of  $i_{ds,2nl}$  (the second order distortion of  $i_{ds}$ ) as a function of  $g_{m1,1}/I_{D,1}$ . Since  $I_{D,1}$  is constant,  $c_1$ , the self-gain of  $M_1$ , is increased as the  $g_m/I_D$  of  $M_1$  increases (Fig. 5a). Figure 5b, Fig. 5c and Fig. 5d are significant because they show that  $g_{m2,1}$  is the primary contributor to  $i_{ds,2nl}$  among the second-order nonlinear parameters. Since the contribution of  $i_{ds,2nl}$  due to  $g_{m2,1}$  increases with  $g_{m1,1}/I_{D,1}$  (Fig. 5d), the gain (Eq. 11) of the envelope detector can be increased by increasing the  $g_m/I_D$  of  $M_1$  at the expense of reducing the transit frequency of  $M_1$ , and hence the frequency range of the envelope detector.

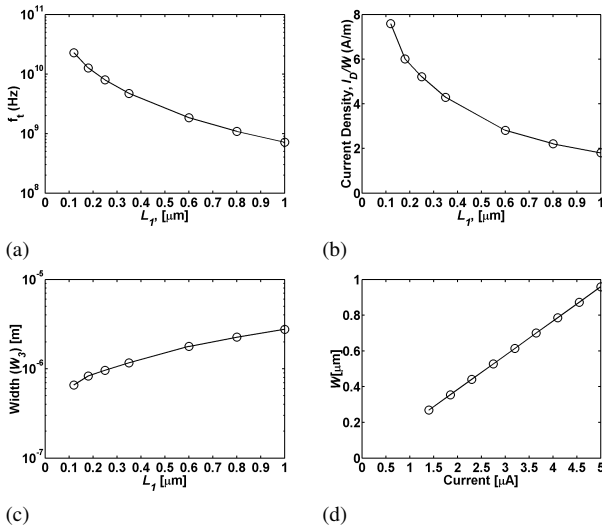


Fig. 4. Current density,  $W_1$ ,  $f_{T1}$  plotted as a function of  $L_1$ .  $I_{D,1}$  is  $5 \mu\text{A}$  and  $g_m/I_D = 20 \text{ S/A}$  for (a)-(c).  $W_1$  is plotted as a function of  $I_{D,1}$  in (d) assuming that  $g_m/I_D$  for  $M_1$  is  $20 \text{ S/A}$ ,  $L_1=250 \text{ nm}$ ,  $V_{DS}=0.6 \text{ V}$  and  $V_{SB}=0.0 \text{ V}$ .

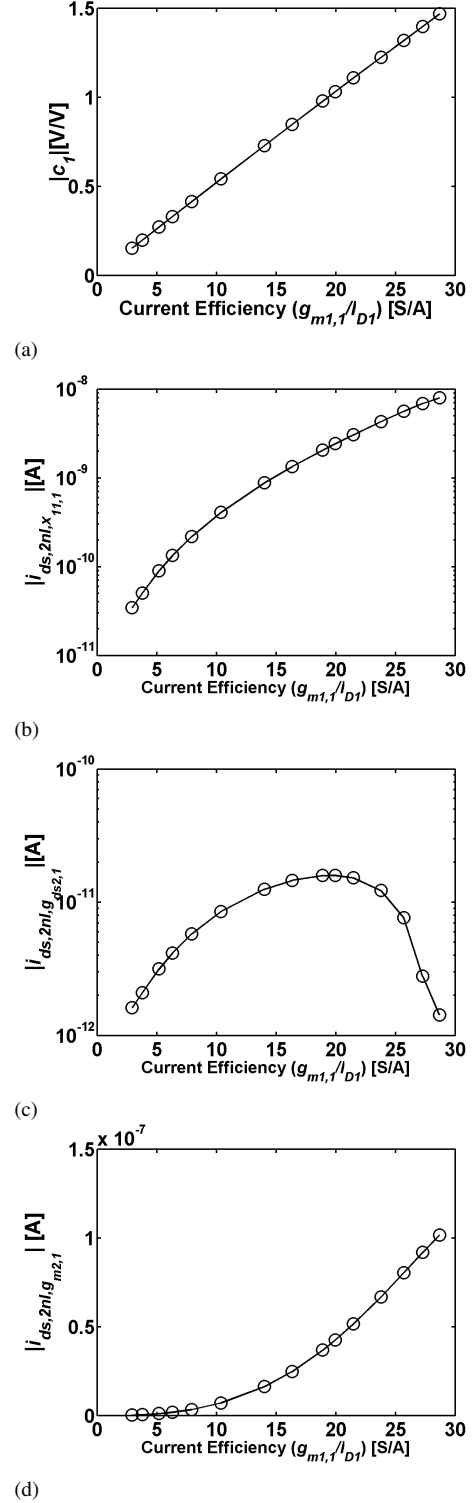


Fig. 5. (a)  $c_1$  versus  $g_m/I_D$  of  $M_1$ . (b)  $x_{11,1}$  contribution to  $i_{ds,2nl}$ . (c)  $g_{ds2,1}$  contribution to  $i_{ds,2nl}$ . (d)  $g_{m2,1}$  contribution to  $i_{ds,2nl}$ .  $i_{ds,2nl}$  represents the second order distortion of  $i_{ds}$ .  $L_1$  is  $250 \text{ nm}$  and  $I_{D,1}$  is  $1.5 \mu\text{A}$ .

#### V. SIMULATION RESULTS

##### A. Nonlinearity of $M_2$

It is assumed in Sec. III that  $M_1$  is primarily responsible for the nonlinear operation of the envelope detector. To verify

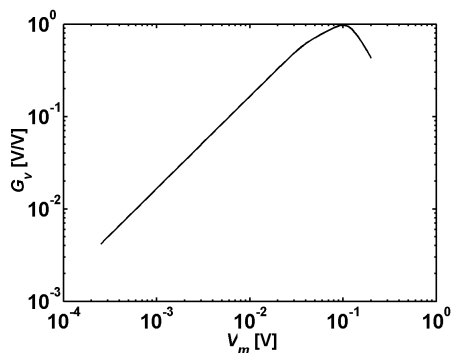


Fig. 6. Conversion gain as a function of  $v_m$ .

this assumption, a sinusoid with a magnitude of 20 mV and a frequency of 1 kHz is applied to  $v_{in}$ . A distortion summary is generated at  $v_{out}$  using SpectreRF. The total second order distortion at  $v_{out}$  is 6.598 mV with a contribution of 6.483 mV from  $M_1$ , a contribution of 0.115 mV from  $M_2$ .  $M_3$  and  $M_4$  do not contribute any second order distortion.  $M_1$  is primarily responsible for the second order nonlinearity at  $v_{out}$ .

### B. $g_m/I_D$ Analysis

The second order nonlinearity contribution of  $M_1$  is calculated by applying a sinusoidal tone with a 20 mV magnitude at  $v_{in}$ .  $v_{op,2nl}$  is computed using (7) and compared with that obtained using the Period Steady State (PSS) analysis. The second order distortion computed using the  $g_m/I_D$  method is 8.06 mV and the second order distortion computed using PSS is 6.48 mV.

### C. Dependence on Input Amplitude

Equation (7) shows that  $v_{op,2nl}$  is proportional to  $v_m^2$ . The conversion gain ( $G_v$ ) for an envelope detector can be defined by dividing  $v_{op,2nl}$  by  $v_m$ .

$$G_v = \frac{v_{op,2nl}}{v_m} = -\frac{R_L}{2}(g_{m2,1} + g_{ds2,1}c_1^2 + x_{11}c_1)v_m \quad (11)$$

Equation (11) shows that  $G_v$  is proportional to  $v_m$ . Figure 6 shows the PSS simulation of  $G_v$  as a function of  $v_m$ .  $G_v$  is proportional to  $v_m$  for  $v_m \leq 100$  mV. Since the drain current ( $i_{ds}$ ) is approximated by a two-dimensional Taylor series in (1), the approximation becomes less accurate as  $v_{gs}$  increases in magnitude [2]. As  $v_m$  exceeds 100 mV,  $G_v$  is reduced as the Taylor series approximation becomes less accurate.

### D. Frequency Dependence

The two-dimensional Taylor series approximation ignores frequency dependence introduced by reactive elements. While this approach may be sufficient for low frequency circuits, the approximation becomes less accurate as frequency increases. At higher frequencies, the frequency dependence of reactive components can be calculated. In order to gauge the frequency dependence of the envelope detector, the input frequency of the sinusoid is swept from 1 kHz to 1 GHz. Figure 7 shows that  $G_v$  remains flat up to 100 MHz.

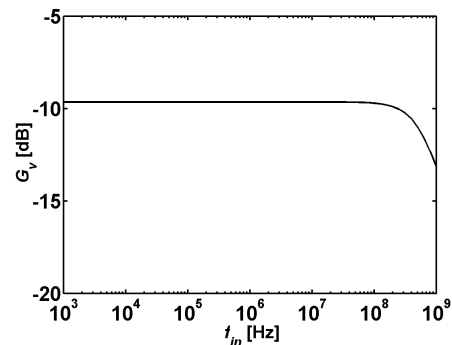


Fig. 7. Frequency dependence of  $G_v$ .

## VI. CONCLUSION

In this paper, we derive an expression that captures second order distortion generated at the output of an envelope detector. We explore the design space to optimize the conversion gain. We show that by systematically working through various design parameters, a 3  $\mu$ A envelope detector can be designed in 0.13  $\mu$ m CMOS process.

## REFERENCES

- [1] F. Silveira, D. Flandre, and P. G. A. Jespers, "A  $g_m/I_D$  Based Methodology for the Design of CMOS Analog Circuits and Its Application to the Synthesis of a Silicon-on-Insulator Micropower OTA," *IEEE J. Solid-State Circuits*, vol.31, no. 9, pp. 1314-1319, Sept. 1996.
- [2] J. Ou and F. Farahmand, "Transconductance/drain current based distortion analysis for analog CMOS integrated circuits," *New Circuits and Systems Conference (NEWCAS), 2012 IEEE 10th International, Montreal, QC, 2012*, pp. 61-64.
- [3] P. G. A. Jespers and B. Murmann, "Calculation of MOSFET distortion using the transconductance-to-current ratio ( $g_m/I_D$ )," *2015 IEEE International Symposium on Circuits and Systems (ISCAS), Lisbon, 2015*, pp. 529-532.
- [4] I.M. Filanovsky and L.B. Oliveira, "Using 'Reconciliation' Model for Calculation of Harmonics in a MOS Transistor Stage Operating in Moderate Inversion," *2016 IEEE International Symposium on Circuits and Systems (ISCAS), Montreal, 2016*.
- [5] W. Sansen, "Analog Design Essentials", Springer, 2008, ch. 18, pp. 521-522.
- [6] S. Blaakmeer, E. A. M. Klumperink, D. M. W. Leenaerts, and B. Nauta, "Wideband Balun-LNA With Simultaneous Output Balancing, Noise-Canceling and Distortion-Canceling", *IEEE J. Solid-State Circuits*, Vol. 43, No.6, June 2008.
- [7] XiongChuan Huang, P. Harpe, G. Dolmans, H. de Groot and J. R. Long, "A 780 to 950 MHz, 64 to 146  $\mu$ W Power-Scalable Synchronized-Switching OOK Receiver for Wireless Event-Driven Applications," *IEEE Journal of Solid-State Circuits*, vol. 49, no. 5, pp. 1135-1147, May 2014.
- [8] S. Moazzeni, M. Sawan and G. E. R. Cowan, "An Ultra-Low-Power Energy-Efficient Dual-Mode Wake-Up Receiver," *IEEE Transactions on Circuits and Systems I: Regular Papers*, vol. 62, no. 2, pp. 517-526, Feb. 2015.
- [9] M. Zgaren and M. Sawan, "A Low-Power Dual-Injection-Locked RF Receiver With FSK-to-OOK Conversion for Biomedical Implants," *IEEE Transactions on Circuits and Systems I: Regular Papers*, vol. 62, no. 11, pp. 2748-2758, Nov. 2015.
- [10] J. Borremans, L. D. Loch, P. Wambacq and Y. Rolain, "Nonlinearity Analysis of Analog/RF Circuits Using Combined Multisine and Volterra Analysis," *2007 Design, Automation and Test in Europe Conference and Exhibition, Nice, 2007*, pp. 1-6.